DNS of thermocapillary migration of a bi-dispersed suspension of droplets *

Néstor Balcázar-Arciniega[1][0000−0003−0776−2086], Joaquim Rigola[1][0000−0002−6685−3677], and Assensi Oliva[1][0000−0002−2805−4794]

[1] Heat and Mass Transfer Technological Center (CTTC), Universitat Politècnica de Catalunya-BarcelonaTech (UPC). Colom 11, 08222, Terrassa (Barcelona), Spain
nestor.balcazar@upc.edu, nestorbalcazar@yahoo.es

Abstract. The multiple markers unstructured conservative level-set method for two-phase flow with variable surface tension is applied in the Direct Numerical Simulation of thermocapillary-migration of a bi-dispersed suspension of droplets. Surface tension is a function of temperature on the interface. Consequently, the called Marangoni stresses induced by temperature gradients on the interface lead to a coupling of the momentum transport equation with the thermal energy transport equation. The finite-volume method on three-dimensional collocated unstructured meshes discretizes the transport equations. Interface capturing is carried out by the unstructured conservative level-set method. The multiple marker approach avoids fluid particles' numerical and potentially unphysical coalescence. The classical fractional-step projection method solves the pressure-velocity coupling. Unstructured flux limiters schemes solve the convective term of transport equations. Adaptive mesh refinement is incorporated to optimize computational resources. Verifications, validations and numerical findings are reported.

Keywords: Unstructured Conservative Level-Set Method · Unstructured Flux-Limiters · Finite-Volume Method · Unstructured Meshes · Adaptive Mesh Refinement · Variable Surface Tension · Thermocapillarity.

1 Introduction

Interfacial phenomena induced by variable surface tension, e.g., thermocapillary or surfactants, are frequent in nature and industry. Diverse engineering systems, from nuclear reactors to unit operations and chemical reactors, from combustion engines to wastewater treatment plants, entail bubbles or droplets inside another fluid phase with complex interfacial physics. This work focuses on the Marangoni migration (Thermocapillarity) of droplets, an interfacial phenomenon induced by a nonuniform temperature distribution on the fluid interface. Because the surface tension is a function of the temperature,

* The principal author, N. Balcázar-Arciniega, as a Serra-Húnter Lecturer (UPC-LE8027), acknowledges the Catalan Government for the financial support through this program. The computing time granted by the RES (IM-2023-1-0003, IM-2022-2-0009, IM-2021-3-0013, IM-2020-2-0002) and PRACE 14th Call (2016153612) on the supercomputer MareNostrum IV based in Barcelona - Spain, is thankfully acknowledged. The financial support of the MINECO - Spain (PID2020-115837RB-100) is acknowledged.

ICCS Camera Ready Version 2023
To cite this paper please use the final published version:
DOI: 10.1007/978-3-031-36030-5_25

surface tension gradients arise. Consequently, shear stresses on the interface induce the migration of droplets in the direction of the temperature gradient. Beyond its scientific importance, thermocapillary migration is essential in microgravity environments [41] and micro-devices [22].

Experimental research on bubble swarms or suspension of droplets with complex interfacial physics, e.g., thermocapillary, is constrained by optical access. In contrast, analytical methods can be applied only for particular cases with a substantial simplification of physics. Consequently, the development of computational methods [35,48] for complex multiphase flows is well justified. In this framework, many methods have been designed for Direct Numerical Simulation (DNS) of gas-liquid multiphase flow [35,48]. For instance, level-set (LS) [34,44,25], Volume of Fluid (VoF) [26,38,49,36], coupled VoF-LS [43,42,10], conservative level-set (CLS) [33,9,16], and front-tracking (FT) [50,47]. Although a similar idea is shared in designing these methods, their numerical implementations on structured or unstructured meshes present significative differences [16,10,6,9].

Further efforts to extend the aforementioned interface capturing/tracking methods for two-phase flows with variable surface tension have been reported, e.g., thermocapillary effects. For instance, Balcazar et al.[14] reported a level-set model for thermocapillary migration of individual and multiple droplets. [32,31] researched the thermocapillary migration of multiple deformable droplets by using front-tracking simulations. [29,39] reported DNS of thermal Marangoni effects at deformable interfaces based on the volume-of-fluid method. [53,52] reported front-tracking simulations of an isolated spherical drop in thermocapillary migration for low and high Marangoni numbers. Two- and three-dimensional level-set simulations of thermocapillary migration of droplets were reported by [54,20]. A front-tracking method for insoluble and soluble surfactants was introduced by [30]. The previous works have reported remarkable numerical and physical findings. Nevertheless, many other configurations and flow conditions have to be explored yet. Consequently, this research is a systematic effort toward designing computational methods for two-phase flow with complex interface physics, i.e., thermocapillary-driven two-phase flow, using the unstructured conservative level-set (UCLS) method proposed by Balcazar et al.[16,18,7,4,8,14,6,9]. Contributions of this work include the incorporation of novel adaptive mesh refinement and unstructured conservative level-set method for thermocapillary migration of droplets. In addition, the DNS of the thermocapillary-driven motion of a bi-dispersed suspension of droplets is presented on three-dimensional fixed meshes.

The organization of this paper is described as follows: The mathematical formulation and numerical methods are introduced in Section 2. Section 3 reports numerical experiments. Conclusions are outlined in Section 4.

2 Mathematical Formulation and Numerical Methods

2.1 One fluid formulation for incompressible two-phase flow

The one-fluid formulation [49,36] solves the Navier-Stokes equations for the dispersed phase (Ω_d) and continuous phase (Ω_c), using the multi-marker UCLS approach [16,18]:

ICCS Camera Ready Version 2023
To cite this paper please use the final published version:
DOI: 10.1007/978-3-031-36030-5_25

$$\frac{\partial}{\partial t}(\rho \mathbf{v}) + \nabla \cdot (\rho \mathbf{v}\mathbf{v}) = -\nabla p + \nabla \cdot \mu \left(\nabla \mathbf{v}\right) + \nabla \cdot \mu (\nabla \mathbf{v})^T + (\rho - \rho_0)\mathbf{g} + \mathbf{f}_\sigma, \quad (1)$$

$$\nabla \cdot \mathbf{v} = 0, \quad (2)$$

where p is the pressure, $\mathbf{v}$ is the fluid velocity, $\mathbf{g}$ denotes the gravitational acceleration, ρ is the fluid density, μ is the dynamic viscosity, $\mathbf{f}_\sigma$ refers to the surface tension force per unit volume concentrated on the interface (Γ), subscripts d and c refer to the dispersed and continuous phases. Density and viscosity are constant. Nevertheless, a jump discontinuity arises on the interface: $\mu = \mu_c H_c + \mu_d H_d$, $\rho = \rho_c H_c + \rho_d H_d$. The Heaviside step function (H_c) is one in Ω_c and zero in Ω_d. On the other hand, $H_d = 1 - H_c$. In case periodic boundary conditions are set in the y-axis (parallel to $\mathbf{g}$), a force $-\rho_0 \mathbf{g}$ should be included in Eq.(1) [16,5,6]. In that case, $\rho_0 = V_\Omega^{-1} \int_\Omega (\rho_c H_c + \rho_d H_d)\, dV$.

2.2 The multi-marker UCLS method

The Unstructured Conservative Level-Set (UCLS) approach proposed by Balcazar et al. [16,9] is used for interface capturing in the framework of the finite volume method. Furthermore, the multiple markers UCLS method [16,4,5,14,6,18] is adopted to circumvent the numerical coalescence of fluid particles. In this context, a modified level-set function [16,14,9] represents each marker, $\phi_i = \frac{1}{2}\left(\tanh\left(\frac{d_i}{2\varepsilon}\right) + 1\right)$, where ε sets the thickness of the interface profile, and d_i is a signed distance function [34,45]. The ith UCLS advection equation is computed in the conservative form:

$$\frac{\partial \phi_i}{\partial t} + \nabla \cdot \phi_i \mathbf{v} = 0, \;\; i = \{1, 2, ..., N_m - 1, N_m\}, \quad (3)$$

N_m is the number of UCLS markers, which equals the number of bubbles or droplets. To maintain a constant and sharp UCLS profile, a re-initialization equation [9] is solved:

$$\frac{\partial \phi_i}{\partial \tau} + \nabla \cdot \phi_i (1 - \phi_i)\mathbf{n}_i^0 = \nabla \cdot \varepsilon \nabla \phi_i, \;\; i = \{1, 2, ..., N_m - 1, N_m\}. \quad (4)$$

Here, $\mathbf{n}_i^0$ denotes the interface normal unit vector evaluated at $\tau = 0$. At the control volume Ω_P, $\varepsilon_P = 0.5(h_P)^\alpha$ with $\alpha = 0.9$, h_P refers to the local grid size [16,14,9]. Eq.(4) is computed for the pseudo-time τ up to the steady state. Interface curvatures κ_i and normal vectors $\mathbf{n}_i$ are computed as follows [16,6,9]: $\kappa_i = -\nabla \cdot \mathbf{n}_i$, $\mathbf{n}_i = \frac{\nabla \phi_i}{||\nabla \phi_i||}$.

2.3 Marangoni force

The Continuous Surface Force (CSF) model [19] is adopted for computing the surface tension force ($\mathbf{f}_\sigma$, Eq.(1)). This model has been extended to the multiple marker UCLS approach by Balcazar et al. [6,14,5,16,18]:

$$\mathbf{f}_\sigma = \sum_{i=1}^{N_m} (\mathbf{f}_{\sigma,i}^{(n)} + \mathbf{f}_{\sigma,i}^{(t)}). \quad (5)$$

ICCS Camera Ready Version 2023
To cite this paper please use the final published version:
DOI: 10.1007/978-3-031-36030-5_25

Here, the interface tangential component $\mathbf{f}_{\sigma,i}^{(t)}$, is the so-called Marangoni force [23], defined as follows:

$$\begin{aligned}\mathbf{f}_{\sigma,i}^{(t)} &= \nabla_{\Gamma_i}\sigma(T)\delta_{\Gamma,i}^{s} = (\nabla\sigma(T) - \mathbf{n}_i(\mathbf{n}_i\cdot\nabla\sigma(T)))\delta_{\Gamma,i}^{s} \\ &= (\nabla\sigma(T) - \mathbf{n}_i(\mathbf{n}_i\cdot\nabla\sigma(T)))||\nabla\phi_i||. \end{aligned} \tag{6}$$

The regularized Dirac delta function $\delta_{\Gamma,i}^{s} = ||\nabla\phi_i||$ [16,9,5,18] is concentrated on the interface. Note that the tangential component of the gradient operator is $\nabla_{\Gamma_i} = \nabla - \mathbf{n}_i(\mathbf{n}_i\cdot\nabla)$. Furthermore, $\sigma = \sigma(T)$ denotes the equation of state for the surface tension coefficient. On the other hand, the normal component of the surface tension force, $\mathbf{f}_{\sigma,i}^{(n)}$, is calculated as follows:

$$\mathbf{f}_{\sigma,i}^{(n)} = \sigma\kappa_i\mathbf{n}_i\delta_{\Gamma,i}^{s}, = \sigma\kappa_i\mathbf{n}_i||\nabla\phi_i||, = \sigma\kappa_i\nabla\phi_i. \tag{7}$$

This force is perpendicular to the interface (Γ_i), whereas k_i is the curvature.

2.4 Equation of state $\sigma = \sigma(T)$ and energy equation

The properties of the vapour and liquid phases for a specific fluid become similar as its critical temperature is reached. Indeed, an increment of temperature reduces the surface tension, i.e., $\partial\sigma(T)/\partial T = \sigma_T$ with $\sigma_T < 0$. For most fluids, a linear equation of state for surface tension is expected: $\sigma = \sigma(T) = \sigma_0 + \sigma_T(T - T_0)$, with $\sigma_0 = \sigma(T_0)$. As a consequence, the Marangoni force (Eq.(6)) for linear $\sigma(T)$ is written as:

$$\mathbf{f}_{\sigma,i}^{(t)} = \mathbf{f}_{\sigma,i}^{(t)}(T) = (\sigma_T\nabla T - \sigma_T\mathbf{n}_i(\mathbf{n}_i\cdot\nabla T))||\nabla\phi_i||. \tag{8}$$

The following energy transport equation [14] address the evolution of the temperature:

$$\rho c_p\left(\frac{\partial T}{\partial t} + \nabla\cdot(\mathbf{v}T)\right) = \nabla\cdot(\lambda\nabla T). \tag{9}$$

Here, $\lambda = \lambda_d H_d + \lambda_c H_c$ is the thermal conductivity, and $c_p = c_{p,d}H_d + c_{p,c}H_c$ is the specific heat capacity. Subindex d and c denotes the dispersed and continuous phases.

2.5 Regularization of physical properties

This research employs a regularization of physical properties $\{\mu, \lambda, \rho c_p\}$ proposed by [14] for thermocapillary migration of droplets: $\rho = \rho_d H_d^s + \rho_c H_c^s$, $\mu^{-1} = \mu_d^{-1}H_d^s + \mu_c^{-1}H_c^s$, $(\rho c_p) = (\rho c_p)_d H_d^s + (\rho c_p)_c H_c^s$, $\lambda^{-1} = \lambda_d^{-1}H_d^s + \lambda_c^{-1}H_c^s$. Further details can be found in our previous research [16,14,6].

2.6 Numerical methods

Transport equations are discretized by the finite-volume method on 3D collocated unstructured meshes [16]. The convective term of level-set advection equation (Eq.(3)), momentum transport equation (Eq.(1)) and energy transport equation (Eq.(9)) is explicitly calculated at the cell-faces by the unstructured flux-limiter schemes proposed

ICCS Camera Ready Version 2023
To cite this paper please use the final published version:
DOI: 10.1007/978-3-031-36030-5_25

by Balcazar et al.[16,9]. Consequently, the convective term in the cell Ω_P is written as follows $(\nabla \cdot \beta\psi\mathbf{v})_P = V_P^{-1}\sum_f \beta_f\psi_f(\mathbf{v}_f \cdot \mathbf{A}_f)$. Here, $\mathbf{A}_f = ||\mathbf{A}_f||\mathbf{e}_f$ is the area vector, subindex f refers to the cell-faces, $\mathbf{e}_f$ is a unit-vector pointing outside the local cell Ω_P, and V_P denotes the volume of Ω_P. Furthermore,

$$\psi_f = \psi_{C_p} + \frac{1}{2}\mathrm{L}(\theta_f)(\psi_{D_p} - \psi_{C_p}), \tag{10}$$

where $\theta_f = (\psi_{C_p} - \psi_{U_p})/(\psi_{D_p} - \psi_{C_p})$ is the monitor variable and $L(\theta_f)$ is the flux limiter function. Furthermore, subindex C_p denotes the upwind point, subindex U_p refers to the far-upwind point, and subindex D_p denotes the downwind point, according to the stencil proposed for the UCLS method [16]. Multiple flux limiters have been implemented on the UCLS solver [16], some of them are remarked [46,24,28]:

$$L(\theta_f) \equiv \begin{cases} \max\{0, \min\{2\theta_f, 1\}, \min\{2, \theta_f\}\} & \text{SUPERBEE,} \\ \max\{0, \min\{4\theta_f, 0.75 + 0.25\theta_f, 2\}\} & \text{SMART,} \\ (\theta_f + |\theta_f|)/(1 + |\theta_f|) & \text{VANLEER,} \\ 0 & \text{UPWIND,} \\ 1 & \text{CD,} \end{cases} \tag{11}$$

SUPERBEE limiter is used unless otherwise stated. The finite-volume discretization of the compressive term in the re-initialization equation (Eq. (4)) is performed at the cell Ω_P as proposed by [16]: $(\nabla \cdot \phi_i(1-\phi_i)\mathbf{n}_i^0)_P = \frac{1}{V_P}\sum_f(\phi_i(1-\phi_i))_f\mathbf{n}_{i,f}^0 \cdot \mathbf{A}_f$. In addition, $(\phi_i(1-\phi_i))_f$ and $\mathbf{n}_{i,f}^0$ are approximated by linear interpolation.

Discretization of the diffusive term in transport equations is performed by the central difference scheme [16]. On the other hand, linear interpolation (with a weighting factor of 0.5) [16] is used to approximate the cell-face values unless otherwise stated. The weighted least-squares method [16,18,7,9] computes the gradients at the cell centroids. The pressure-velocity coupling is solved with the fractional-step projection method [21,36,49]. Indeed, a predictor velocity ($\mathbf{v}_P^*$) is calculated in the first step:

$$\frac{\rho_P\mathbf{v}_P^* - \rho_P^0\mathbf{v}_P^0}{\Delta t} = \mathbf{C}_{\mathbf{v},P}^0 + \mathbf{D}_{\mathbf{v},P}^0 + (\rho_P - \rho_0)\mathbf{g} + \mathbf{f}_{\sigma,P}, \tag{12}$$

Here, subindex P denotes the local control volume (Ω_P), superindex 0 refers to the previous time-step, $\mathbf{C}_\mathbf{v} = -\nabla\cdot(\rho\mathbf{v}\mathbf{v})$, and $\mathbf{D}_\mathbf{v} = \nabla\cdot\mu\nabla\mathbf{v} + \nabla\cdot\mu(\nabla\mathbf{v})^T$. After imposing the incompressibility constraint ($(\nabla\cdot\mathbf{v})_P = 0$) in the corrector step (Eq. (14)), a Poisson equation for the pressure field is obtained:

$$\left(\nabla\cdot\left(\frac{\Delta t}{\rho}\nabla p\right)\right)_P = (\nabla\cdot\mathbf{v}^*)_P\,,\ \mathbf{e}_{\partial\Omega}\cdot\nabla p|_{\partial\Omega} = 0. \tag{13}$$

A linear system results from the finite volume approximation of Eq.(13), which is computed by a preconditioned (Jacobi pre-conditioner) conjugate gradient method [27,51]. Here $\partial\Omega$ refers to the boundary of Ω, excluding regions with periodic conditions where information of the corresponding periodic nodes is used [16,6]. In the next step, an updated velocity ($\mathbf{v}_P$) is calculated as follows:

$$\frac{\rho_P\mathbf{v}_P - \rho_P\mathbf{v}_P^*}{\Delta t} = -(\nabla p)_P. \tag{14}$$

ICCS Camera Ready Version 2023
To cite this paper please use the final published version:
DOI: 10.1007/978-3-031-36030-5_25

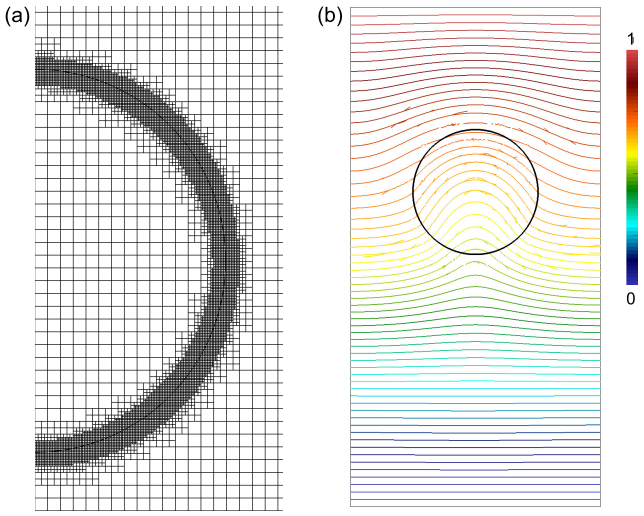

Fig. 1. Thermocapillary migration of a single droplet, $\mathbf{g} = \mathbf{0}$. (a) Adaptive mesh refinement (AMR) around the interface. The maximum grid size is $h_{max} = L_x/60$, and the minimum grid size is $h_{min} = h_{max}/2^4$. (b) Temperature isocontours.

Furthermore, to avoid pressure-velocity decoupling on collocated meshes [37] and to fulfil the incompressibility constraint, a cell-face velocity $\mathbf{v}_f$ is interpolated [14,16]. Consistently with $\mathbf{v}_f$, the volume flux ($\mathbf{v}_f \cdot \mathbf{A}_f$), normal velocity ($\mathbf{v}_f \cdot \mathbf{e}_f$) or a compatible variable is used to calculate the convective term of transport equations (see appendix A of [14] for example). The reader is referred to [16,7,18] for an example of a global algorithm for complex interfacial physics and further details on the finite-volume discretization.

3 Numerical Experiments

Validations, verifications and extensions of the UCLS method [16,7,9,11,5] have been systematically reported, including: the gravity-driven motion of single bubbles [9,6,5,3,2], Thermocapillary migration of single and multiple droplets on fixed unstructured meshes [14,15], falling droplets [8], gravity-driven bubbly flows [12,5,16,17,18], the bouncing collision of a droplet against a fluid-fluid interface [12], binary droplet collision [12], deformation of droplets under shear stresses [10], primary atomization of a liquid [40], mass transfer in bubble swarms [18,4,16,17], and saturated liquid-vapour phase change [7]. A comparison of the UCLS method [9,6,14] and unstructured coupled VoF-LS method [10] is performed in [8]. Consequently, this research is a further systematic step in thermocapillary-driven two-phase flows.

ICCS Camera Ready Version 2023
To cite this paper please use the final published version:
DOI: 10.1007/978-3-031-36030-5_25

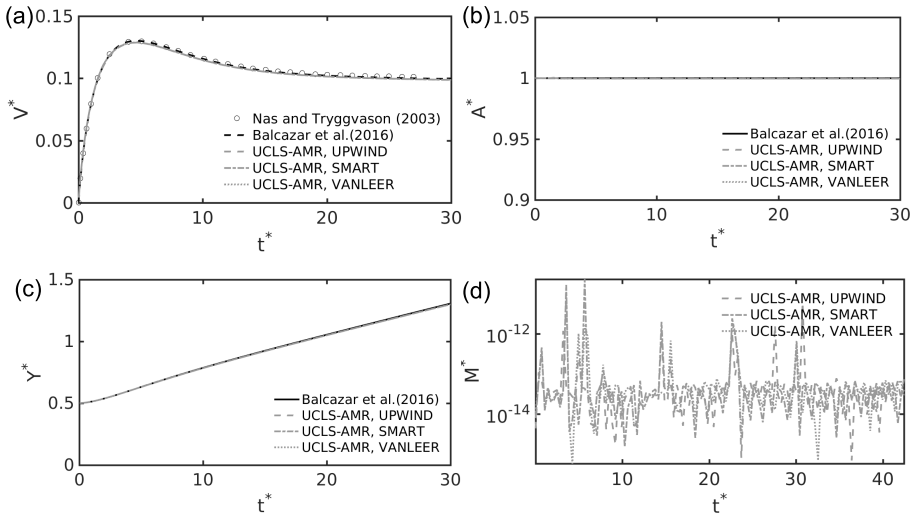

Fig. 2. Effect of flux-limiter schemes (UPWIND, SMART, VANLEER) on thermocapillary migration of a single droplet, $\mathbf{g} = \mathbf{0}$. Comparison of present simulations (AMR-UCLS) against front tracking simulations of Nas and Tryggvason (2003) [32], and conservative level-set simulations of Balcazar et al.(2016) [13] on fixed meshes. Here $t^* = t/t_r$. (a) Migration velocity $V^* = (\mathbf{e}_y \cdot \mathbf{v})U_r^{-1}$. (b) Dimensionless droplet surface $A^* = A(t)/A(0)$, $A(t) = \int_\Omega ||\nabla\phi|| dV$. (c) Position of the droplet centre on the y-axis $Y^* = y/L_x$. (d) Mass conservation $M^* = (M(t) - M(0))/M(0)$, $M(t) = \int_\Omega H_d^s dV$.

The following dimensionless numbers characterize the thermocapillary migration of droplets:

$$\text{Ma} = \frac{|\sigma_T|||\nabla T_\infty||d^2\rho_c c_{p,c}}{4\mu_c\lambda_c}, \text{Re} = \frac{|\sigma_T|||\nabla T_\infty||d^2\rho_c}{4\mu_c^2},$$
$$\text{Ca} = \frac{|\sigma_T|||\nabla T_\infty||d}{2\sigma_0}, \eta_\beta = \frac{\beta_c}{\beta_d}. \tag{15}$$

where Ca is the capillary number, Ma is the Marangoni number, Re is the Reynolds number, η_β denotes the physical property ratio, $\beta = \{\rho, \mu, \lambda, c_p\}$, $\nabla T_\infty = ((T_h - T_c)/L_y)\mathbf{e}_y$, T_h denotes the temperature at the top boundary (hot), and T_c denotes the temperature at the bottom boundary (cold), as depicted in Figure 1b. On the other hand, $T_r = ||\nabla T_\infty||(0.5d)$ defines the reference temperature, $U_r = |\sigma_T|||\nabla T_\infty||(0.5d)/\mu_c$ is the reference velocity, and $t_r = 0.5d/U_r$ is the reference time.

3.1 Thermocapillary migration of a single droplet

This test case was reported by [32] in the framework of the front-tracking method. Furthermore, it has been successfully computed through the UCLS method on fixed unstructured meshes by Balcazar et al.[14]. In what follows the UCLS method [16,14,9,18]

ICCS Camera Ready Version 2023
To cite this paper please use the final published version:
DOI: 10.1007/978-3-031-36030-5_25

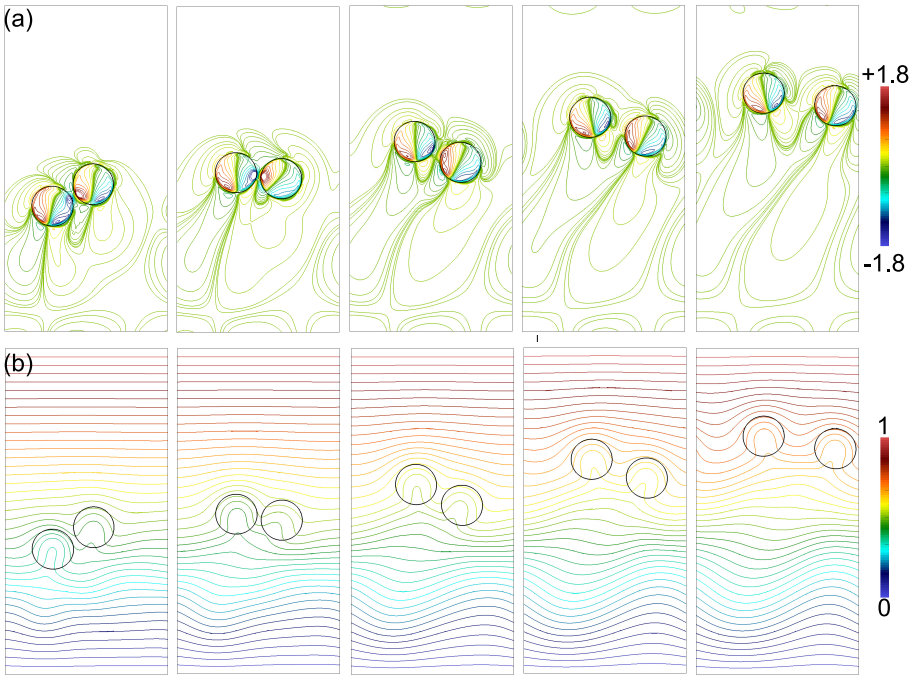

Fig. 3. Thermocapillary interaction of two droplets $\mathbf{g} = \mathbf{0}$. $Re = 60$, $Ma = 60$, $Ca = 0.0416\bar{6}$, $\eta_\rho = \eta_\mu = \eta_{c_p} = \eta_\lambda = 2$. Uniform hexahedral mesh with grid size $h = d/48$. (a) Vorticity contours ($(\nabla \times \mathbf{v}) \cdot \mathbf{e}_z$). (b) Temperature contours.

for two-phase flow with variable surface tension is coupled to a hexahedral Adaptive Mesh Refinement strategy (AMR) [3]. The hexahedral AMR technique was introduced by [1] for single-phase turbulent flows. In a further step, [3] extended and optimized this technique for rising bubbles at high Reynolds numbers (wobbling-regime) in the framework of the UCLS two-phase flow solver proposed by Balcazar et al.[16,8,9].

The computational setup consists of a rectangle domain (Ω) extending $L_x = 4d$ in the x direction and $L_y = 8d$ in the y direction, whereas d is the droplet diameter. As an initial condition, the droplet centroid is located above the bottom wall at a distance d. The top and bottom walls are no-slip boundaries with temperature T_h and $T_c < T_h$, respectively. On the other hand, the periodic boundary condition is applied to lateral boundaries (x-axis). The material property ratios η_ρ, η_μ, η_{c_p} and η_λ are set to 0.5, whereas the dimensionless parameters are chosen as Re $= 5$, Ma $= 20$, and Ca $= 0.016\bar{6}$. Figure 1 shows an instantaneous result for the temperature field induced by thermocapillary migration and details on the AMR applied to the droplet interface. Figure 2 illustrates that numerical results computed by the AMR-UCLS method are in close agreement with those reported by [32] and [14] on fixed meshes. Moreover, Figure 2d shows excellent mass conservation of fluid phases.

ICCS Camera Ready Version 2023
To cite this paper please use the final published version:
DOI: 10.1007/978-3-031-36030-5_25

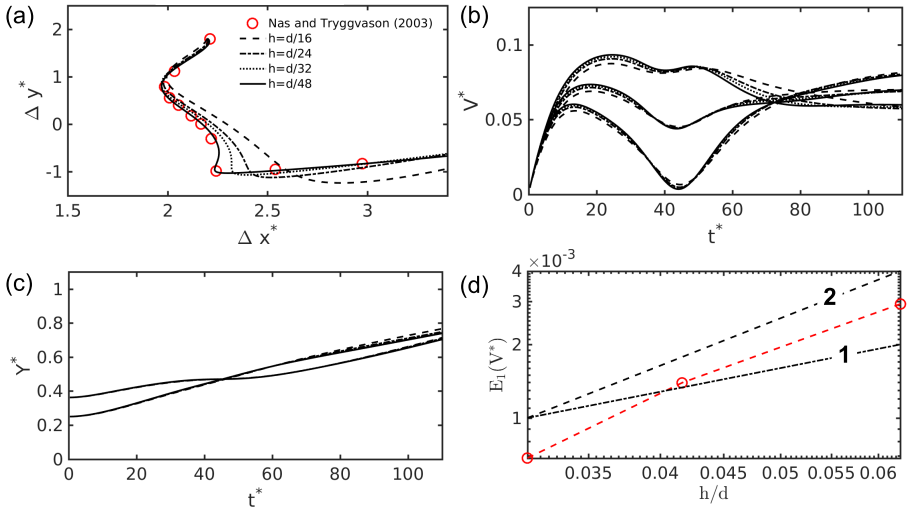

Fig. 4. Thermocapillary interaction of two droplets, with $\mathbf{g} = \mathbf{0}$, $Ma = 60$, $Re = 60$, $Ca = 0.0416\bar{6}$, $\eta_\rho = 2$, $\eta_\mu = 2$, $\eta_{c_p} = 2$, $\eta_\lambda = 2$. Lines denote the present numerical results with grid size $h = \{d/16, d/24, d/32, d/48\}$. Red symbols depict the front-tracking simulation reported by [32]. (a) Vertical versus horizontal separation distance. (b) Migration velocity. (c) Position of the droplet centre on the y-axis $Y^* = y/L_y$. (d) Order of convergence: The red line denotes present simulations. Black lines for first-order and second-order convergence. $E_1(V^*) = N^{-1}\sum_{i=1}^{N} ||V_i^* - V_{i,ref}^*||$, $V_{i,ref}^*$ refers to numerical results for the finest mesh $h = d/48$.

3.2 Thermocapillary interaction of two droplets

This test case was reported by [32] in the framework of the front-tracking method. Here, this case is computed by the UCLS method on fixed meshes. The computational setup consists of a rectangle domain (Ω), which extends $L_x = 4\,d$ on the x-axis, $L_y = 8\,d$ on the y-axis, and $L_z = h$, where h is the grid size. Ω is discretized by $\{8192, 18432, 32768, 73728\}$ uniform hexahedral cells. Accordingly, the grid sizes are $h = \{d/16, d/24, d/32, d/48\}$. The material properties ratios are $\eta_\rho = 2$, $\eta_\mu = 2$, $\eta_\lambda = 2$, $\eta_{c_p} = 2$. Further dimensionless parameters are set to Ma $= 60$, Ca $= 0.0416\bar{6}$, and Re $= 60$. The initial droplet centroids are $(x/d, y/d) = (0.95, 2.0)$, and $(x/d, y/d) = (2.05, 2.9)$. The droplets are circular cylinders of diameter d at $t = 0$. Concerning the boundary conditions, periodic conditions are set in the x direction. On the other hand, the top and bottom walls are no-slip boundaries. Temperatures at the top and bottom boundaries (y-axis) are T_t and T_b, respectively, with $T_t > T_b$.

Fig. 3 depicts the isotherms and vorticity contours ($\mathbf{e}_z \cdot \nabla \times \mathbf{v}$) for thermocapillary interaction of the two droplets. Additionally, Fig. 4a depicts the vertical separation distance of droplets against its horizontal separation distance. As the grid is refined, numerical results using the UCLS method converge toward the front-tracking simulation reported by [32]. Fig. 4b illustrates the migration velocity V^*, whereas grid convergence

ICCS Camera Ready Version 2023
To cite this paper please use the final published version:
DOI: 10.1007/978-3-031-36030-5_25

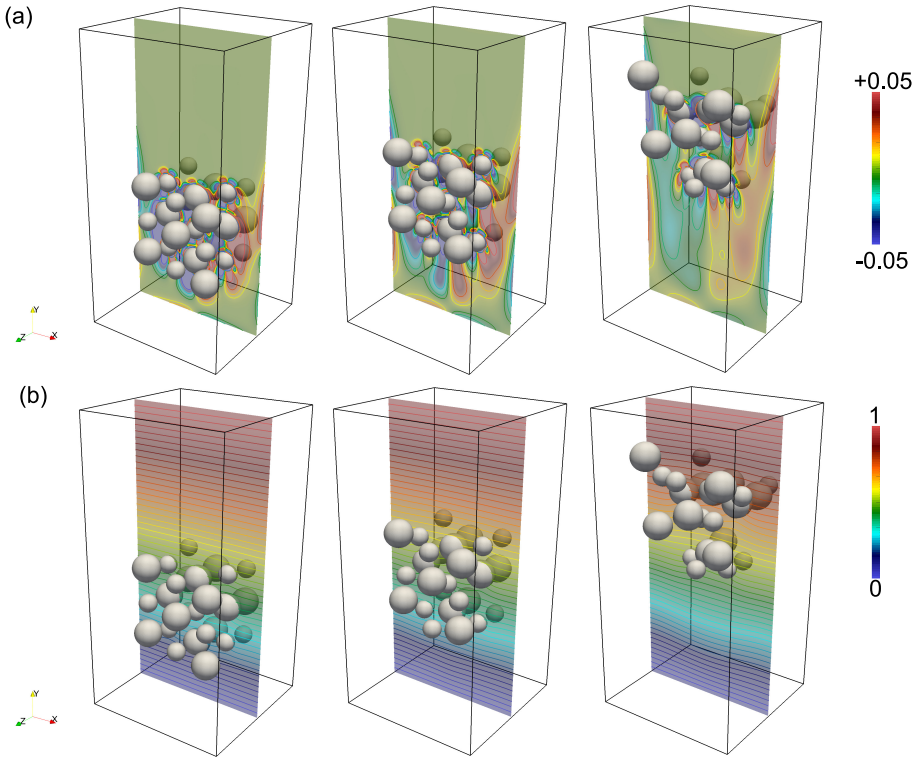

Fig. 5. Thermocapillary interaction of a bi-dispersed suspension of 27 droplets ($\mathbf{g} = \mathbf{0}$), distributed as 13 droplets with diameter d, and 14 droplets with diameter d^*. Re $= 80$, Ma $= 10$, Ca $= 0.0416\bar{6}$, $\eta_\rho = \eta_\mu = \eta_{c_p} = \eta_\lambda = 2$, $d/d^* = 1.5$. Uniform hexahedral mesh with grid size $h = d/48$, equivalent to 27648000 control volumes. Simulation performed on 1536 CPU cores. (a) Vorticity contours ($(\nabla \times \mathbf{v}) \cdot \mathbf{e}_z$) at $t^* = t/t_r = \{16.4, 32.8, 65.7\}$. (b) Temperature contours.

(second order) is demonstrated in Fig. 4d. An acceleration and deceleration period is experienced by both droplets, which is evidenced by the overshoot in their migration velocities. After that, one of the droplets reaches a quasi-steady state ($t^* \geq 60$), whereas the other presents a new acceleration stage ($t^* \geq 40$).

3.3 Thermocapillary migration of a bi-dispersed suspension of droplets

The multi-marker UCLS method performs the DNS of thermocapillary migration of a bi-dispersed suspension of droplets. Ω is a rectangular channel of size $L_y = 10.66\,d$ in the y axis, and $(L_x, L_z) = (5.33\,d, 5.33\,d)$ on the plane $x - z$. Ω is discretized by 27648000 uniform hexahedral control volumes ($240 \times 240 \times 480$ grid points), with grid size $h = d/45$. At $t = 0$, 27 droplets are set near the bottom boundary, following a random pattern (Fig. 5a). The suspension of droplets consists of 13 droplets of diameter

ICCS Camera Ready Version 2023
To cite this paper please use the final published version:
DOI: 10.1007/978-3-031-36030-5_25

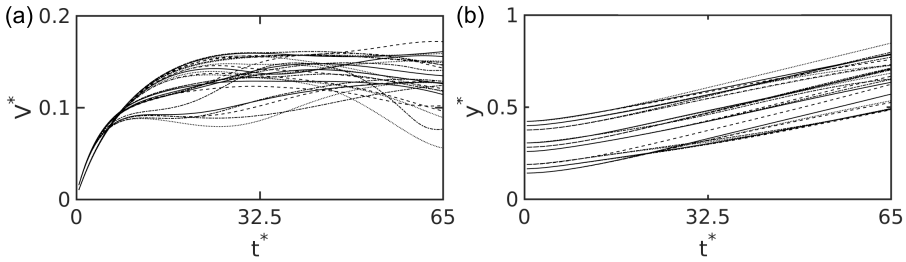

Fig. 6. Thermocapillary interaction of a bi-dispersed suspension of 27 droplets $\mathbf{g} = \mathbf{0}$, distributed as 13 droplets with diameter d, and 14 droplets with diameter d^*. Re $= 80$, Ma $= 10$, Ca $= 0.0416\bar{6}$, $\eta_\rho = \eta_\mu = \eta_{c_p} = \eta_\lambda = 2$, $d/d^* = 1.5$. Uniform hexahedral mesh with grid size $h = d/48$, equivalent to 27648000 control volumes. Simulation performed on 1536 CPU cores. (a) Dimensionless migration velocity $V^* = \mathbf{e}_y \cdot \mathbf{v}_{c,i}/U_r$, $\mathbf{v}_{c,i}$ is the droplet velocity. (b) Dimensionless vertical position, $y^* = \mathbf{e}_y \cdot \mathbf{x}_{c,i}/L_y$, $\mathbf{x}_{c,i}$ is the droplet centroid.

d and 14 droplets of diameter d^*. The diameter ratio is $d/d^* = 1.5$. Dimensionless numbers are defined concerning the droplet diameter d, as outlined in Fig. 5 and Fig. 6. The fluids are initially quiescent, and the temperature increases linearly from the bottom wall to the top wall. The adiabatic boundary condition is applied to lateral walls. On the other hand, the temperature at the top and bottom boundaries are T_h and T_c, respectively, with $T_h > T_c$. The no-slip boundary condition applies to all the boundaries. Fig. 5 show instantaneous vorticity and temperature contours as the droplets migrate to the hot wall. Fig. 6 depicts the migration velocity of each droplet and the vertical position of droplet centroids.

4 Conclusions

The multi-marker UCLS method for two-phase flow with variable surface tension has been applied to the thermocapillary migration of droplets. Validations and verifications include the Marangoni migration of a single droplet using AMR and the interaction of two droplets on fixed meshes. The unstructured flux-limiters schemes proposed by Balcazar et al.[16,9], to discretize the convective term of transport equations in the framework of the UCLS method, minimize the so-called numerical diffusion and avoid numerical oscillations at the interface. Altogether, numerical schemes lead to a robust and accurate numerical method for complex thermocapillary-driven two-phase flow on 3D collocated unstructured meshes.

References

1. Antepara, O., Lehmkuhl, O., Borrell, R., Chiva, J., Oliva, A.: Parallel adaptive mesh refinement for large-eddy simulations of turbulent flows. Computers and Fluids **110**, 48–61 (mar 2015). https://doi.org/10.1016/j.compfluid.2014.09.050, `https://linkinghub.elsevier.com/retrieve/pii/S0045793014003958`

ICCS Camera Ready Version 2023
To cite this paper please use the final published version:
DOI: 10.1007/978-3-031-36030-5_25

2. Antepara, O., Balcázar, N., Oliva, A.: Tetrahedral adaptive mesh refinement for twophase flows using conservative levelset method. International Journal for Numerical Methods in Fluids **93**(2), 481–503 (2021). https://doi.org/10.1002/fld.4893, https://onlinelibrary.wiley.com/doi/10.1002/fld.4893
3. Antepara, O., Balcázar, N., Rigola, J., Oliva, A.: Numerical study of rising bubbles with path instability using conservative level-set and adaptive mesh refinement. Computers and Fluids **187**, 83–97 (2019). https://doi.org/10.1016/j.compfluid.2019.04.013, https://linkinghub.elsevier.com/retrieve/pii/S0045793018306297
4. Balcazar, N., Antepara, O., Rigola, J., Oliva, A.: DNS of Drag-Force and Reactive Mass Transfer in Gravity-Driven Bubbly Flows. In: García-Villalba, M., Kuerten, H., Salvetti, M. (eds) Direct and Large Eddy Simulation XII. DLES 2019. ERCOFTAC Series, vol 27. Springer, Cham pp. 119–125 (2020). https://doi.org/10.1007/978-3-030-42822-8$_1$6, http://link.springer.com/10.1007/978-3-030-42822-8_16
5. Balcazar, N., Castro, J., Rigola, J., Oliva, A.: DNS of the wall effect on the motion of bubble swarms. Procedia Computer Science **108**, 2008–2017 (2017). https://doi.org/10.1016/j.procs.2017.05.076, https://linkinghub.elsevier.com/retrieve/pii/S1877050917306142
6. Balcazar, N., Lehmkuhl, O., Jofre, L., Oliva, A.: Level-set simulations of buoyancy-driven motion of single and multiple bubbles. International Journal of Heat and Fluid Flow **56** (2015). https://doi.org/10.1016/j.ijheatfluidflow.2015.07.004
7. Balcazar, N., Rigola, J., Oliva, A.: Unstructured Level-Set Method For Saturated Liquid-Vapor Phase Change. In: WCCM-ECCOMAS 2020. Volume 600 - Fluid Dynamics and Transport Phenomena. pp. 1–12 (2021). https://doi.org/10.23967/wccm-eccomas.2020.352, https://www.scipedia.com/public/Balcazar_et_al_2021a
8. Balcazar, N., Castro, J., Chiva, J., Oliva, A.: DNS of falling droplets in a vertical channel. International Journal of Computational Methods and Experimental Measurements **6**(2), 398–410 (nov 2017). https://doi.org/10.2495/CMEM-V6-N2-398-410, http://www.witpress.com/doi/journals/CMEM-V6-N2-398-410
9. Balcazar, N., Jofre, L., Lehmkuhl, O., Castro, J., Rigola, J.: A finite-volume/level-set method for simulating two-phase flows on unstructured grids. International Journal of Multiphase Flow **64**, 55–72 (2014). https://doi.org/10.1016/j.ijmultiphaseflow.2014.04.008, https://linkinghub.elsevier.com/retrieve/pii/S030193221400072X
10. Balcazar, N., Lehmkuhl, O., Jofre, L., Rigola, J., Oliva, A.: A coupled volume-of-fluid/level-set method for simulation of two-phase flows on unstructured meshes. Computers and Fluids **124**, 12–29 (2016). https://doi.org/10.1016/j.compfluid.2015.10.005, https://linkinghub.elsevier.com/retrieve/pii/S0045793015003394
11. Balcazar, N., Lehmkuhl, O., Jofre, L., Rigola, J., Oliva, A.: A coupled volume-of-fluid/level-set method for simulation of two-phase flows on unstructured meshes. Computers & Fluids **124**, 12–29 (2016). https://doi.org/10.1016/j.compfluid.2015.10.005, https://linkinghub.elsevier.com/retrieve/pii/S0045793015003394
12. Balcazar, N., Lehmkuhl, O., Rigola, J., Oliva, A.: A multiple marker level-set method for simulation of deformable fluid particles. International Journal of Multiphase Flow **74**, 125–142 (2015). https://doi.org/10.1016/j.ijmultiphaseflow.2015.04.009, https://linkinghub.elsevier.com/retrieve/pii/S0301932215001019
13. Balcazar, N., Oliva, A., Rigola, J.: A level-set method for thermal motion of bubbles and droplets. Journal of Physics: Conference Series **745**, 032113 (2016). https://doi.org/10.1088/1742-6596/745/3/032113
14. Balcazar, N., Rigola, J., Castro, J., Oliva, A.: A level-set model for thermocapillary motion of deformable fluid particles. International Journal of Heat and Fluid Flow **62**, 324–343 (dec 2016). https://doi.org/10.1016/j.ijheatfluidflow.2016.09.015, https://linkinghub.elsevier.com/retrieve/pii/S0142727X16301266

ICCS Camera Ready Version 2023
To cite this paper please use the final published version:
DOI: 10.1007/978-3-031-36030-5_25

15. Balcazar Arciniega, N., Rigola, J., Oliva, A.: A level-set model for two-phase flow with variable surface tension: Thermocapillary and surfactants. In: 8th European Congress on Computational Methods in Applied Sciences and Engineering. CIMNE (2022). https://doi.org/10.23967/eccomas.2022.011, https://www.scipedia.com/public/Balcazar_Arciniega_et_al_2022a
16. Balcazar-Arciniega, N., Antepara, O., Rigola, J., Oliva, A.: A level-set model for mass transfer in bubbly flows. International Journal of Heat and Mass Transfer **138**, 335–356 (2019). https://doi.org/10.1016/j.ijheatmasstransfer.2019.04.008
17. Balcazar-Arciniega, N., Rigola, J., Oliva, A.: DNS of Mass Transfer from Bubbles Rising in a Vertical Channel. Lecture Notes in Computer Science (including subseries Lecture Notes in Artificial Intelligence and Lecture Notes in Bioinformatics) **11539 LNCS**, 596–610 (2019). https://doi.org/10.1007/978-3-030-22747-0$_4$5, http://link.springer.com/10.1007/978-3-030-22747-0_45
18. Balcazar-Arciniega, N., Rigola, J., Oliva, A.: DNS ofmass transfer in bi-dispersed bubble swarms. In: Computational Science ICCS 2022. ICCS 2022. Lecture Notes in Computer Science, vol 13353. Springer, Cham **13353**, 284–296 (2022). https://doi.org/10.1007/978-3-031-08760-8$_2$4, https://link.springer.com/10.1007/978-3-031-08760-8_24
19. Brackbill, J.U., Kothe, D.B., Zemach, C.: A continuum method for modeling surface tension. Journal of Computational Physics **100**(2), 335–354 (1992). https://doi.org/10.1016/0021-9991(92)90240-Y, https://linkinghub.elsevier.com/retrieve/pii/002199919290240Y
20. Brady, P.T., Herrmann, M., Lopez, J.M.: Confined thermocapillary motion of a three-dimensional deformable drop. Physics of Fluids **23**(2), 022101 (feb 2011). https://doi.org/10.1063/1.3529442, http://aip.scitation.org/doi/10.1063/1.3529442
21. Chorin, A.J.: Numerical Solution of the Navier-Stokes Equations. Mathematics of Computation **22**(104), 745 (1968). https://doi.org/10.2307/2004575, https://www.jstor.org/stable/2004575?origin=crossref
22. Darhuber, A.A., Troian, S.M.: PRINCIPLES OF MICROFLUIDIC ACTUATION BY MODULATION OF SURFACE STRESSES. Annual Review of Fluid Mechanics **37**(1), 425–455 (jan 2005). https://doi.org/10.1146/annurev.fluid.36.050802.122052, https://www.annualreviews.org/doi/10.1146/annurev.fluid.36.050802.122052
23. Deen, W.: Analysis of Transport Phenomena. OXFORD UNIV PR (2011)
24. Gaskell, P.H., Lau, A.K.C.: Curvature-compensated convective transport: SMART, A new boundedness- preserving transport algorithm. International Journal for Numerical Methods in Fluids **8**(6), 617–641 (1988). https://doi.org/10.1002/fld.1650080602, http://doi.wiley.com/10.1002/fld.1650080602
25. Gibou, F., Fedkiw, R., Osher, S.: A review of level-set methods and some recent applications. Journal of Computational Physics **353**, 82–109 (jan 2018). https://doi.org/10.1016/j.jcp.2017.10.006, https://linkinghub.elsevier.com/retrieve/pii/S0021999117307441
26. Hirt, C., Nichols, B.: Volume of fluid (VOF) method for the dynamics of free boundaries. Journal of Computational Physics **39**(1), 201–225 (jan 1981). https://doi.org/10.1016/0021-9991(81)90145-5, https://linkinghub.elsevier.com/retrieve/pii/0021999181901455
27. Karniadakis, G.E., Kirby II, R.M.: Parallel Scientific Computing in C++ and MPI. Cambridge University Press (jun 2003). https://doi.org/10.1017/CBO9780511812583, https://www.cambridge.org/core/product/identifier/9780511812583/type/book

ICCS Camera Ready Version 2023
To cite this paper please use the final published version:
DOI: 10.1007/978-3-031-36030-5_25

28. LeVeque, R.J.: Finite Volume Methods for Hyperbolic Problems (2002). https://doi.org/10.1017/cbo9780511791253
29. Ma, C., Bothe, D.: Direct numerical simulation of thermocapillary flow based on the Volume of Fluid method. International Journal of Multiphase Flow **37**(9), 1045–1058 (nov 2011). https://doi.org/10.1016/j.ijmultiphaseflow.2011.06.005, https://linkinghub.elsevier.com/retrieve/pii/S0301932211001273
30. Muradoglu, M., Tryggvason, G.: A front-tracking method for computation of interfacial flows with soluble surfactants. Journal of Computational Physics **227**(4), 2238–2262 (feb 2008). https://doi.org/10.1016/j.jcp.2007.10.003, https://linkinghub.elsevier.com/retrieve/pii/S002199910700438X
31. Nas, S., Muradoglu, M., Tryggvason, G.: Pattern formation of drops in thermocapillary migration. International Journal of Heat and Mass Transfer **49**(13-14), 2265–2276 (jul 2006). https://doi.org/10.1016/j.ijheatmasstransfer.2005.12.009, https://linkinghub.elsevier.com/retrieve/pii/S0017931006000093
32. Nas, S., Tryggvason, G.: Thermocapillary interaction of two bubbles or drops. International Journal of Multiphase Flow **29**(7), 1117–1135 (jul 2003). https://doi.org/10.1016/S0301-9322(03)00084-3, https://linkinghub.elsevier.com/retrieve/pii/S0301932203000843
33. Olsson, E., Kreiss, G.: A conservative level set method for two phase flow. Journal of Computational Physics **210**(1), 225–246 (nov 2005). https://doi.org/10.1016/j.jcp.2005.04.007, https://linkinghub.elsevier.com/retrieve/pii/S0021999105002184
34. Osher, S., Sethian, J.A.: Fronts propagating with curvature-dependent speed: Algorithms based on Hamilton-Jacobi formulations. Journal of Computational Physics **79**(1), 12–49 (nov 1988). https://doi.org/10.1016/0021-9991(88)90002-2, https://linkinghub.elsevier.com/retrieve/pii/0021999188900022
35. Prosperetti, A., Tryggvason, G.: Computational Methods for Multiphase Flow. Cambridge University Press, Cambridge (2007). https://doi.org/10.1017/CBO9780511607486
36. Prosperetti, A., Tryggvason, G.: Computational Methods for Multiphase Flow. Cambridge University Press, Cambridge (2007). https://doi.org/10.1017/CBO9780511607486
37. Rhie, C.M., Chow, W.L.: Numerical study of the turbulent flow past an airfoil with trailing edge separation. AIAA Journal **21**(11), 1525–1532 (1983). https://doi.org/10.2514/3.8284, https://arc.aiaa.org/doi/10.2514/3.8284
38. Rider, W.J., Kothe, D.B.: Reconstructing Volume Tracking. Journal of Computational Physics **141**(2), 112–152 (apr 1998). https://doi.org/10.1006/jcph.1998.5906, https://linkinghub.elsevier.com/retrieve/pii/S002199919895906X
39. Samareh, B., Mostaghimi, J., Moreau, C.: Thermocapillary migration of a deformable droplet. International Journal of Heat and Mass Transfer **73**, 616–626 (jun 2014). https://doi.org/10.1016/j.ijheatmasstransfer.2014.02.022
40. Schillaci, E., Antepara, O., Balcázar, N., Serrano, J.R., Oliva, A.: A numerical study of liquid atomization regimes by means of conservative level-set simulations. Computers and Fluids **179**, 137–149 (2019). https://doi.org/10.1016/j.compfluid.2018.10.017, https://linkinghub.elsevier.com/retrieve/pii/S0045793018307801
41. Subramanian, R., Balasubramaniam, R., Clark, N.: Motion of Bubbles and Drops in Reduced Gravity. Applied Mechanics Reviews **55**(3), B56–B57 (may 2002). https://doi.org/10.1115/1.1470685, https://asmedigitalcollection.asme.org/appliedmechanicsreviews/article/55/3/B56/456871/Motion-of-Bubbles-and-Drops-in-Reduced-Gravity
42. Sun, D., Tao, W.: A coupled volume-of-fluid and level set (VOSET) method for computing incompressible two-phase flows. International Journal of Heat and Mass Transfer **53**(4),

ICCS Camera Ready Version 2023
To cite this paper please use the final published version:
DOI: 10.1007/978-3-031-36030-5_25

645–655 (jan 2010). https://doi.org/10.1016/j.ijheatmasstransfer.2009.10.030, https://linkinghub.elsevier.com/retrieve/pii/S0017931009005717
43. Sussman, M., Puckett, E.G.: A Coupled Level Set and Volume-of-Fluid Method for Computing 3D and Axisymmetric Incompressible Two-Phase Flows. Journal of Computational Physics **162**(2), 301–337 (aug 2000). https://doi.org/10.1006/jcph.2000.6537, https://linkinghub.elsevier.com/retrieve/pii/S0021999100965379
44. Sussman, M., Smereka, P., Osher, S.: A Level Set Approach for Computing Solutions to Incompressible Two-Phase Flow. Journal of Computational Physics **114**(1), 146–159 (sep 1994). https://doi.org/10.1006/jcph.1994.1155, https://linkinghub.elsevier.com/retrieve/pii/S0021999184711557
45. Sussman, M., Smereka, P., Osher, S.: A Level Set Approach for Computing Solutions to Incompressible Two-Phase Flow. Journal of Computational Physics **114**(1), 146–159 (sep 1994). https://doi.org/10.1006/jcph.1994.1155, https://linkinghub.elsevier.com/retrieve/pii/S0021999184711557
46. Sweby, P.K.: High Resolution Schemes Using Flux Limiters for Hyperbolic Conservation Laws. SIAM Journal on Numerical Analysis **21**(5), 995–1011 (oct 1984). https://doi.org/10.1137/0721062, http://epubs.siam.org/doi/10.1137/0721062
47. Tryggvason, G., Bunner, B., Esmaeeli, A., Juric, D., Al-Rawahi, N., Tauber, W., Han, J., Nas, S., Jan, Y.J.: A Front-Tracking Method for the Computations of Multiphase Flow. Journal of Computational Physics **169**(2), 708–759 (may 2001). https://doi.org/10.1006/jcph.2001.6726, https://linkinghub.elsevier.com/retrieve/pii/S0021999101967269
48. Tryggvason, G., Scardovelli, R., Zaleski, S.: The volume-of-fluid method. In: Direct Numerical Simulations of GasLiquid Multiphase Flows, pp. 95–132. Cambridge University Press (jan 2001). https://doi.org/10.1017/CBO9780511975264.006, https://www.cambridge.org/core/product/identifier/CBO9780511975264A041/type/book_part
49. Tryggvason, G., Scardovelli, R., Zaleski, S.: Direct numerical simulations of Gas-Liquid multiphase flows (2011). https://doi.org/10.1017/CBO9780511975264
50. Unverdi, S.O., Tryggvason, G.: A front-tracking method for viscous, incompressible, multi-fluid flows. Journal of Computational Physics **100**(1), 25–37 (may 1992). https://doi.org/10.1016/0021-9991(92)90307-K, https://linkinghub.elsevier.com/retrieve/pii/002199919290307K
51. Van der Vorst, H.A., Dekker, K.: Conjugate gradient type methods and preconditioning. Journal of Computational and Applied Mathematics **24**(1-2), 73–87 (nov 1988). https://doi.org/10.1016/0377-0427(88)90344-5, https://linkinghub.elsevier.com/retrieve/pii/0377042788903445
52. Yin, Z., Chang, L., Hu, W., Li, Q., Wang, H.: Numerical simulations on thermocapillary migrations of nondeformable droplets with large Marangoni numbers. Physics of Fluids **24**(9), 092101 (sep 2012). https://doi.org/10.1063/1.4752028, http://aip.scitation.org/doi/10.1063/1.4752028
53. Yin, Z., Li, Q.: Thermocapillary migration and interaction of drops: Two non-merging drops in an aligned arrangement. Journal of Fluid Mechanics **766**, 436–467 (mar 2015). https://doi.org/10.1017/jfm.2015.10, https://www.cambridge.org/core/product/identifier/S0022112015000105/type/journal_article
54. Zhao, J.F., Li, Z.D., Li, H.X., Li, J.: Thermocapillary Migration of Deformable Bubbles at Moderate to Large Marangoni Number in Microgravity. Microgravity Science and Technology **22**(3), 295–303 (sep 2010). https://doi.org/10.1007/s12217-010-9193-x

ICCS Camera Ready Version 2023
To cite this paper please use the final published version:
DOI: 10.1007/978-3-031-36030-5_25